Challenges and limitations using the Integral Transform Method to obtain the impact noise level of timber floors

Simone Conta, Anders Homb
Department of Civil and Environmental Engineering, NTNU, Trondheim, Norway

Summary
The Woodsol project aims at developing long span lightweight floors based on a wood-box concept for timber buildings with high architectural flexibility. The major challenge regarding impact sound insulation is expected to be at low and medium frequencies. The impact noise level of the building element needs to be measured but no building acoustics laboratory offers an opening with a size of 8 to 10 m. For this reason, we intend to use the Integral Transform Method (ITM) to determine the impact noise level. The input to the ITM is the measured vibration velocity on the building element. Based on the spatial Fourier transformation, the ITM can be used to calculate the radiated sound power in the wave number domain. From that, the impact noise level is calculated. The result shall be comparable with results obtained performing measurements according to the relevant standards. Preliminary measurements were performed on a prototype floor. Assessment of the measured vibration levels and calculated impact noise levels will be given. The practical challenges and limitations encountered so far will also be addressed and discussed in this paper.

PACS no. 43.40.+s, 43.58.+z

1. Introduction

This paper describes measurements performed on a Woodsol prototype floor element. The design of the element is based on the wood-box concept. The section of the floor element is shown in figure 1. The upper and bottom plate are laminated veneer lumber of type Kerto-Q, while the stringers are glulam. This type of construction was chosen to fulfil the requirements set by the project. The floor shall span at least 9 m and contribute to the structure of the building with high stiffness. The fire resistance requirements set the minimum thickness of the bottom plate. Goal of the measurements is to asses the acoustic properties of this construction as a starting point for further development.

Considering the lightweight properties of the floor element and its size, the major challenge regarding impact sound insulation is expected to be at low and medium frequencies. Common building acoustics laboratories have openings sizes with dimensions of about 3 m x 4 m. We therefore need to use an alternative measurement method to determine the impact noise level of the floor element. The Integral Transform Method (ITM) is gaining popularity and appeared to be a suitable tool. Although a number of references are available on the ITM, its application is not straightforward and requires an accurate planning of the measurements and a comprehensive analysis of the acquired measurement data. In this paper, after briefly recalling the basic elements of the theory behind the ITM, we present the procedure we followed to set up and carry out the measurements. We will also present preliminary results and some considerations about the validity of the data.

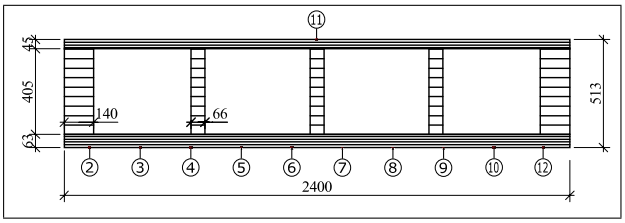

Figure 1. Cross section of the Woodsol floor element under investigation. The numbers indicate the positions of the accelerometers.

2. Theory and procedure

The ITM has its foundation in the wavenumber transform and the description of the plane radiators as sum of plane wave [1]. For the current work following references were mainly used: for the implementation we

referred to the PhD thesis of Mathias Kohrmann [2] while for the measurement setup, the work of Stefan Schoenwald [3] and Christoph Winter [4] have been important sources.
In the following, we shall recall the steps and the equations, which are needed to define a proper measurement setup and implement the method in e.g. Matlab. We will also highlight the elements that are necessary for a reliable measurement setup.

2.1. Basic quantities

We will first recall some relations for a number of basic quantities for easier reference.
The bending wave speed c_B in the material is the governing quantity. We are dealing here with engineered timber products (Kerto-Q) with orthotropic material properties, which means that the bending wave speed is different in the x and y direction (c_{bx}, c_{by}). Following relations hold :

$$c_{bx}(f) = (2\pi f)^{1/2}\left(\frac{B'_x}{\rho h}\right)^{1/4} \tag{1}$$

$$c_{by}(f) = (2\pi f)^{1/2}\left(\frac{B'_y}{\rho h}\right)^{1/4} \tag{2}$$

with f frequency, B bending stiffness of the structure/plate, ρ density of the material and h height of the structure/plate.
The basic relations between wavelength λ, wavenumber k, frequency f and bending wave speed c_b are:

$$k_x = \frac{2\pi}{\lambda_x} \qquad k_y = \frac{2\pi}{\lambda_y} \tag{3}$$

$$\lambda_x f = c_{bx} \qquad \lambda_y f = c_{by} \tag{4}$$

We shall also recall here the relation for the critical frequency f_c:

$$f_c = \frac{c_0^2}{2\pi}\sqrt{\frac{m''}{B'}} \tag{5}$$

2.2. Measurement grid size

The first step in the ITM method is to measure the vibration velocity distribution on the plate. Since the method is essentially based on a 2-D wavenumber transform, the *Shannon*-Criterion (also known as the *Nyquist*-Theorem) sets the requirement on the grid size. Following relations hold between between raster size Δx, Δy, minimum wavelength λ_{min} and maximum frequency f_{max}

$$\Delta x < \frac{\lambda_{min}}{2}, \qquad \Delta y < \frac{\lambda_{min}}{2}, \tag{6}$$

$$f_{max} < \frac{c_{bx}(f_{max})}{2\Delta x} \qquad f_{max} < \frac{c_{by}(f_{max})}{2\Delta y} \tag{7}$$

Since in the ITM the calculations are carried out in frequency steps, it is not necessary to filter the signal before performing the wavenumber transform. Nevertheless it is necessary to check that no strong peaks with their side lobes are too close to the aliasing limits. This can be easily checked in the wavenumber transform spectra.
The conditions on the grid size imply a high number of measurements points. To reduce the measurement time one can use the geometrical symmetry of the test obejct. Symmetry can be used only up to a certain extent. Winter [4] showed that performing the measurements only on 1/4 of the plate led to an overestimation of the radiated sound power, due to the introduced leakage. Performing the measurements on 1/2 deck might lead to acceptable results, but this needs to be confirmed.
The frequency range of interest for this work is 20 Hz to 200 Hz. Due to the lack of experience with the method and the uncertainties in determining c_{bx} and c_{by}, the raster size was set to 24 cm in x direction and 30 cm in y direction. This should allow to obtain reliable measurements data up to at least 400 Hz.
In the table I, we list several key quantities, compared with similar experiments found in literature. To determine c_b, we used the tabulated Young modulus and density values for Kerto-Q combined with the actual geometry of the deck for the calculation of the bending stiffness. This is a rather rough approach and we shall verify later if it was appropriate or not.

2.3. Calculation of the radiated sound power

At each point of the grid the vibration velocity is converted from the time domain to the frequency domain using a common Fourier Transform. The input data to the integral transform method are now available and can be processed using a two dimensional Fourier Transform (the wavenumber transform) to obtain the radiated sound power. According to [2], the frequency dependent radiated sound power $P(f)$ can be calculated from the measured velocity pattern of a plane radiator in the wave number domain with following relation:

$$P(f) = \frac{1}{2}\frac{\rho_A c_A}{4\pi^2}\Re\Bigg[\int_{-\infty}^{\infty}\int_{-\infty}^{\infty} \frac{k_A(f)}{\sqrt{k_A(f)^2 - k_x^2 - k_y^2}}|\hat{v}(k_x, k_y, f)|^2 dk_x dk_y\Bigg] \tag{8}$$

where following symbols are used:

- $P(f)$ radiated sound power at the frequency f,
- ρ_A density and c_A speed of sound in the air,
- $k_A = \frac{2\pi f}{c_A}$ wavenumber of air,
- k_x and k_y the wavenumbers in x and y direction,
- $\hat{v}(k_x, k_y, f)$ the complex vibration velocity distribution in the wavenumber domain.

Table I. Key quantities for the current setup compared to the reference setups.

Ref.	Material, thickness	Raster size		Bending wave speed @ f_{max}		Nyquist frequency		Critical frequency	
		Δx	Δy	c_{bx}	c_{by}	$f_{max,xdir}$	$f_{max,ydir}$	$f_{c,x}$	$f_{c,y}$
-	Kerto-Q, 63 mm	24 cm	30 cm	645 m/s	867 m/s	1350 Hz	1450 Hz	375 Hz	223 Hz
[3]	CLT, 80 mm	11 cm	11 cm	901 m/s	550 m/s	4100 Hz	2500 Hz	584 Hz	955 HZ
[4]	Gypsum board, 2x 12,5mm	25 cm	25 cm	189 m/s		380 Hz		1224 Hz	
[3]	Steel, 1mm	4 cm	3 cm	116 m/s		1500 Hz		12800 Hz	
[2]	Aluminium plate, 2 mm	6 cm	6 cm	162 m/s		1350 Hz		6000 Hz	

It is necessary to transform this analytical expression into a discrete formulation, in order to use it with measurement data (see [2] for details). $P(f)$ assumes the form of a vector $\mathbf{p}$ with dimension $n_f \times 1$, $K(k_x, k_y, f)$ and $\hat{v}(k_x, k_y, f)$ assume the matrix form $\mathbf{K}$ and $\hat{\mathbf{V}}$ with dimensions $M_\alpha \times M_\beta \times n_f$. The individual terms of $\mathbf{p}$ at the frequency step γ have the form:

$$P[\gamma] = \frac{1}{2}\frac{\rho_A c_A}{4\pi^2}\Re\Bigg[\sum_{\alpha=1}^{M_\alpha}\sum_{\beta=1}^{M_\beta} K[\alpha,\beta,\gamma]\cdot|\hat{v}[\alpha,\beta,\gamma]|^2\Delta x^2\Delta y^2\Bigg]\Delta k_x \Delta k_y \quad (9)$$

where following symbols are used:

- α and β coordinates in the wavenumber domain,
- $M_\alpha = z_p\frac{l}{\Delta x}$ and $M_\beta = z_p\frac{w}{\Delta y}$ number of samples in the wavenumber domain,
- z_p zero padding factor (see section 2.4),
- $l \times w$ dimensions of the plate,
- $\Delta k_x = \frac{2\pi}{z_p l}$ and $\Delta k_y = \frac{2\pi}{z_p w}$ the sampling interval in the wavenumber domain.

The terms of the matrix $\mathbf{K}$ are:

$$K[\alpha\beta\gamma] = \frac{k_A[\gamma]^2}{\sqrt{(k_A[\gamma]^2 - k_x[\alpha]^2 - k_y[\beta]^2)}} \quad (10)$$

The derivation of the individual spectral amplitudes $\hat{v}[\alpha,\beta,\gamma]$ from the vibration velocity pattern in the spatial domain $v[r,s,\gamma]$ (with r and s spatial coordinates) is a key point in the procedure. This is done through a two dimensional Fourier Transform on the vibration velocity pattern in the spatial domain for each frequency step.

2.4. Zero padding

Zero padding is a simple technique used in signal processing to increase the length of a measured signal and hence the resolution of a Fourier Transform. It consists in appending zeros to a signal. The zero padding factor z_p is defined as:

$$z_p = \frac{M}{N} \quad (11)$$

where N is the original length of the signal in samples and M the resulting length, after appending the zeros.

It is is very important to notice here, that while using *zero padding* we increase the resolution of the Fourier Transform, but we are not adding any information to the signal. All the information that is available is the one which could be described with the original resolution. The purpose of using the zero padding technique in the ITM is to achieve a better resolution of the boundaries of the plate. The typical side lobes in the wavenumber spectrum are due to the to the finite size of the plate. From a mathematical point of view, they are due to the sinc function corresponding to the square window describing the finite size of the plate. The higher the resolution, the steeper is the sinc function and the sharper is the description of the finite size of the plate. While using the ITM, one has to choose a value of z_p *high enough* to take this effect properly into account. We are showing an example of this in section 4.2.

In addition to this, a high *zero padding* factor is used to solve some numerical issues related to the **K**-matrix [2]. Preliminary checks showed that the value of $z_p = 50$ used in the current analysis was adequate. Nevertheless we shall verify in our further work this choice, by implementing more advanced thechniques as shown in [2].

2.5. Calculation of the impact noise level

The target of this work is to obtain impact noise level data which are comparable with data obtained from measurements carried out according to the standard ISO16283-2 [5]. As a first approximation, we will use the relation that a sound source with sound power L_W generates a sound pressure level L_i under the assumption of diffuse field as follow, [7]:

$$L_i = L_W - 10log\frac{p_{ref}^2 \cdot 55.3 \cdot V}{P_{ref} \cdot 4\rho c^2 \cdot T_{60}} \quad (12)$$

$$= L_W - 10log\frac{V}{V_0} + 10log\frac{T_{60}}{T_0} + 14dB. \quad (13)$$

According to the standard [5], the normalized impact sound pressure level is calculated as:

$$L'_n = L_i + 10log\frac{A}{A_0}. \quad (14)$$

Combining 13 and 14 we obtain a relation that does not depend on V, T and A:

$$L'_n = L_w - 12dB \quad (15)$$

Figure 2. Woodsol floor element installed on air bellows.

Figure 3. Detail of the supporting air bellows.

The measurement standard requires to measure the sound pressure level at a certain distance from the boundaries. Similarly to what is done in the ISO15186 [6], the *Waterhouse correction* [8] can be used to compensate for this effect :

$$W = \frac{\hat{p}_\infty^2}{4\rho_0 c_0} A\left(1 + \frac{Sc_0}{8Vf}\right) \tag{16}$$

Typical values to use these relation were taken from ISO15186 [6].

3. Experimental setup

3.1. Test object

The procedure described above was used to calculate the normalized impact noise level in the current work. The measurements data were collected using an experimental setup which was dedicated to a modal analysis with free-free boundary conditions. The floor element was mounted on air bellows with the rigid body motion having a frequency of about 3 Hz to 5 Hz. Figure 2 shows the floor element mounted in the lab, including a detail of the mountings with the air bellows.

It is mandatory to highlight here that these boundary conditions are not representative for a typical situation in a building and that the radiated sound power is certainly influenced by this situation. While the absolute value of the radiated sound power might be compromised by this aspect, the considerations about the measurement method are still valid.

The sensors position are shown in figure 1 on the cross section of the element. We used a 12-channel OROS analyser and decided to have 10 accelerometers mounted on a line along the y-direction ($\Delta y = 0.24m$). The measurement line was then moved along the x-direction of the floor ($\Delta x = 0.30m$) while keeping one accelerometer (number 11) fixed for phase reference. The measurements were performed on half deck and the calculated radiated sound power then corrected to the full size of the floor element ($+3dB$).

The accelerometers were mounted using special wooden screws to ensure proper connection of the sensor with the structure.

3.2. Excitation

We used following excitation types: impact hammer and tapping machine. The impact hammer gives the possibility to measure the force and evaluate the transfer functions. The tapping machine was used with the aim of obtaining sound power levels comparable with the lab measurements. The tapping machine was placed at four different positions following the requirement of ISO 16283-2. The impact hammer was used at the same positions as the tapping machine, hitting at the locations of each hammer of the tapping machine.

3.3. Effect of the direct airborne excitation

The measurements of the vibration velocity were performed with the floor element installed in a large industrial hall. There was no separation between the volume above the floor element and the volume below it. This means that the tapping machine could excite the bottom plate in two ways: the expected structure-borne sound due the impact of the hammers and the vibration propagation through the structure and the unwanted airborne sound excitation of the bottom plate due to the sound pressure radiated directly from the upper plate and propagating through the hall.

Preliminary measurements showed that the vibration level generated by the airborne sound excitation is approximately 10 dB lower than the structure-borne excitation but they also showed that this aspect must be taken into account because it might have a relevant effect. Further work is being carried out to better asses this topic.

4. Preliminary results

4.1. Vibration velocity in the wavenumber domain

In figure 4, we show the vibration velocity $|\hat{v}|^2$ distribution for the frequency steps 32 Hz (first bending

mode), 42 Hz (first transversal mode combined with a torsional mode) and 66 Hz (higher order mode). Note that the measured data were mirrored here for the purpose of visualization. In the figure, the excitation positions are marked with white circles while the current active excitation position is highlighted in red. The results match fairly well the frequencies and mode shapes obtained from the experimental modal analysis performed on the same experimental setup.

In figure 5 and 6, we show the vibration velocity $|\hat{v}|^2$ spectra in the wavenumber domain for the first bending mode (32 Hz) and for the frequency step 42 Hz. The black ellipse in the diagrams represents the bending wave speed at the respective frequency calculated using the tabulated data for Kerto-Q. The white circle represent the wavenumber of air k_{air} for this frequency, while the white area highlights the portion of energy that contributes to the radiated sound power.

In figure 5, the main peaks have coordinates k_y close to 0 and $k_x \approx 0.9$. $k_y \approx 0$ corresponds to the fact that the motion related to this mode is aligned with the x axis of the floor element. Similarly in figure 6, $k_x \approx 0$ due to the fact that the mode is along the y axis. The pattern in figure 6 is less clear then in the previous figure, because at this frequency step two vibrational modes are active and the resolution used is not high enough to distinguish the two modes. Results from the experimental modal analysis performed on the same experimental setup showed the first transversal mode at 42.7 Hz and a torsional mode at 42.1 Hz.

In contrast to the common time/frequency Fourier Transform, it is useful here to present the periodical repetition of the Fourier Transform results. The main peaks indeed are expected to lay on a circle (in the case of an isotropic material) or an ellipse (as here, with an orthotropic material), which has the radius corresponding to the associated wavenumber. Knowing the wavenumber and the frequency, it is possible to calculate the bending wave speed. The currently calculated bending wave speed matches only very roughly the measured data. In our further work, we shall use these data to calculate the bending wave speed for the element following the procedure described in [4] and find an improved estimate of the expected bending wave speed. A typical feature of the wavenumber spectra related to finite vibrating plates are the side lobes of the peaks. In our application, they are of utmost importance because they carry part of the information of the radiated sound power. Indeed only the part of the spectrum within the circle with radius k_A (highlighted with the white shading in the figures) contributes to the sound radiation.

Finally, it is worth pointing out here that one should not expect to see a wavenumber spectrum which is perfectly point-symmetrical around the origin. The input to the wave number transform is indeed the complex velocity field. The wave number transform is essentially a 2-D Fourier transform. For a complex signal its output is not symmetrical around the origin.

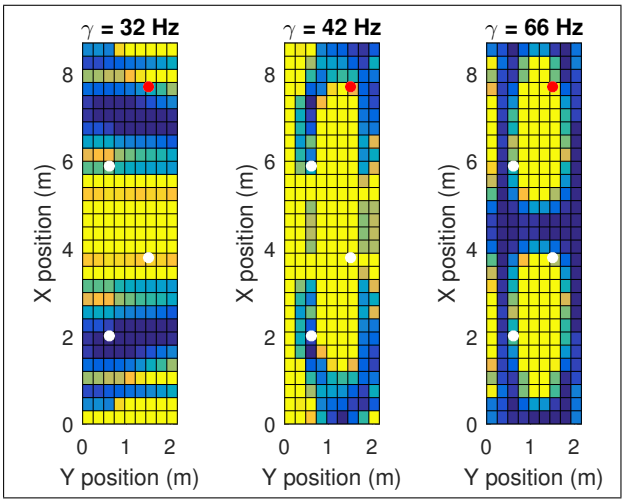

Figure 4. Measured vibration velocity $|v|^2$ distribution. The data were measured on only half deck and are here displayed mirrored. The positions of the tapping machine are marked with the white circles. The red circle indicate the current excitation position.

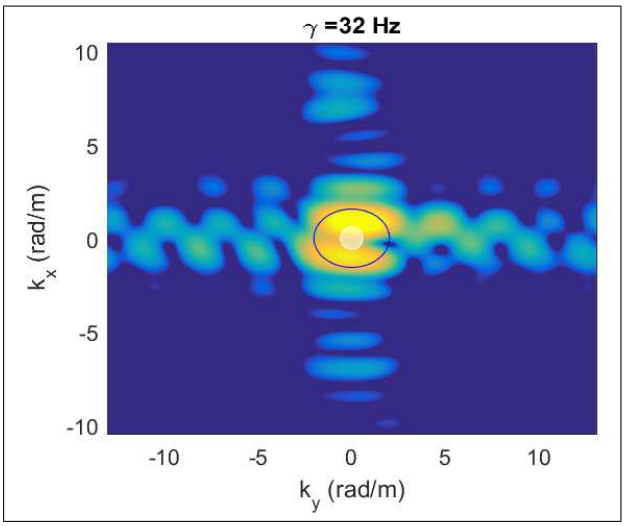

Figure 5. Wavenumber spectrum of the vibration velocity $|v|^2$ for the frequency step $\gamma = 32Hz$. The black ellipse corresponds to the bending wave speed calculated using the tabulated data for Kerto-Q. The white circle represents the wavenumber of air k_{air} for this frequency. The white area inside the circle highlights the contributions to the radiated sound power.

4.2. Effect of zero padding factor

In figure 7 we show the calculated radiated sound power using different values of the *zero padding* factor. With very low values of zero padding ($z_p = 2$) the procedure does not produce stable results because of numerical issues. Increasing z_p from 20 to about 50 the

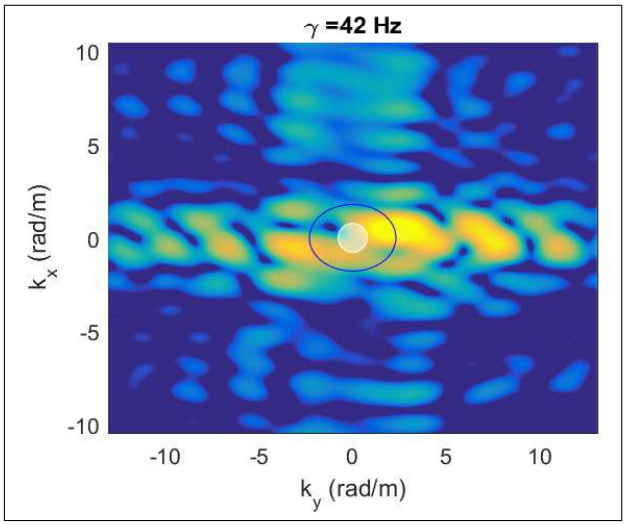

Figure 6. Wavenumber spectrum of the vibration velocity $|v|^2$ for the frequency step $\gamma = 43Hz$. The black ellipse corresponds to the bending wave speed calculated using the tabulated data for Kerto-Q. The white circle represents the wavenumber of air k_{air} for this frequency. The white area highlights the contributions to the radiated sound power.

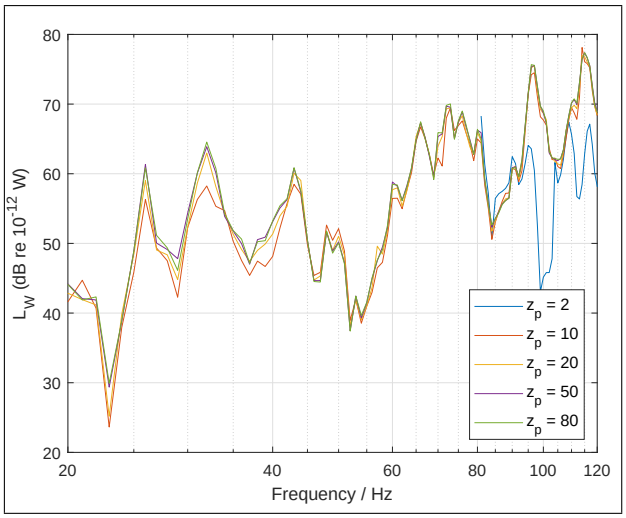

Figure 7. Sound power level calculated with varying *zero padding* factor. The results are shown in the frequency range 20 Hz - 120 Hz for the excitation with tapping machine at one position.

results stabilize at a certain level. Further increasing the zero padding factor does not change the results. For the further calculations we chose to use $z_p = 50$.

4.3. Radiated sound power and impact noise level

The measurement results obtained for the radiated sound power L_W are shown in figure 8. In the diagram the curves obtained for the different excitation positions are shown along with the energetic average. The normalized impact noise level calculated from the energetic average of the measured sound power is shown

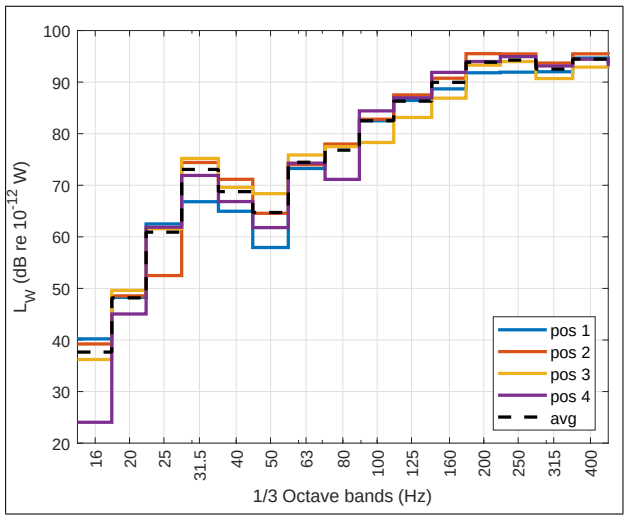

Figure 8. Sound power level calculated from excitation with tapping machine at four different positions.

in figure 9 in 1/3-octave bands up to 400 Hz. The local maxima around the eigenfrequency of the first mode (32 Hz) confirm the expectation that the long span might lead to characteristic features in the spectrum at low frequencies.
For reference we show in the same diagram the normalized impact noise level measured in a lab for three more constructions: two CLT floor elements with similar mass per unit area (m' = 85 kg/m^2 and m' = 89 kg/m^2) [9] and a wood-box construction filled with gravel (m' = 195 kg/m^2) [10]. Unluckily the datasets available only showed frequencies above 50 Hz. The results show that normalized impact noise level for the Woodsol element above 100 Hz is very similar to that for a CLT panel of comparable mass per unit area. The strong differences below 100 Hz could be due to the boundary conditions, the size of the element and the stiffness properties of the design. We will need to confirm this result.

5. Conclusions

In this paper we described the usage of the integral transform method on a prototype floor element. We highlighted the challenges encountered and a few limitations that we faced. All relevant equations, which are needed to define the parameters of the experimental setup and to implement the method in a computer program were given for ease of reference and further usage in the work to come.
The preliminary results were obtained using a tapping machine at four different position as excitation.
From the measured vibration velocity, we calculated the radiated sound power and corrected this so that it should be comparable with data obtained following the measurements procedure described in ISO16283-2. The preliminary results show that above 100 Hz the normalized impact noise level is comparable to that

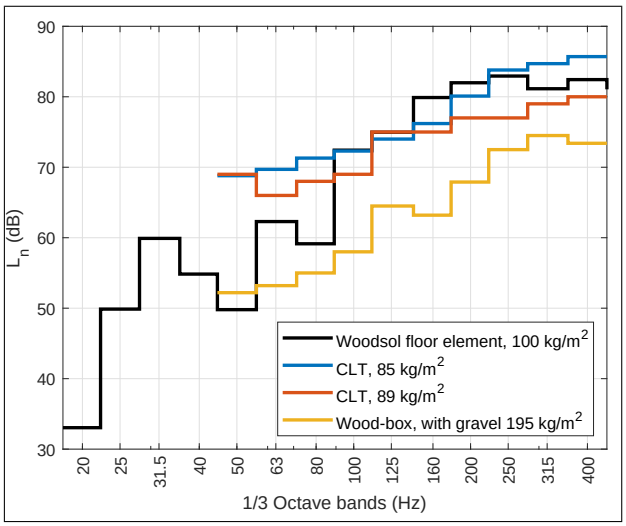

Figure 9. Impact noise level calculated from vibration velocity measurements on the Woodsol floor element (m' = 100 kg/m^2). For comparison three more constructions are shown in the diagram: two CLT floor elements with similar mass per unit area (m' = 85 kg/m^2 and m' = 89 kg/m^2) [9] and a wood-box construction filled with gravel (m' = 195 kg/m^2) [10] .

of a CLT element with similar mass per unit area. At low frequencies, special features were observed that could be due to the boundary conditions, the size of the element and the stiffness properties of the design. Further work is needed to fully understand and validate these results.

Acknowledgement

This project has been carried out within the Woodsol project (http://www.Woodsol.no). Woodsol is funded by the research council of Norway and the consortium partners.

References

[1] Cremer, L., M. Heckl, and B.A. Petersson, Structure-borne sound: structural vibrations and sound radiation at audio frequencies. 2005: Springer.

[2] Kohrmann, M., Numerical Methods for the Vibro-Acoustic Assessment of Timber Floor Constructions, in Ingenieurfakultaet Bau Geo Umwelt (BGU) 2017, Technische Universitaet München.

[3] Schoenwald, S., S. Vallely, and H.-M. Troebs, Advanced methods to determine sound power radiated from planar structures. The Journal of the Acoustical Society of America, 2017. 141(5): p. 3713-3713.

[4] Winter, C., Messtechnische Untersuchung leichter Deckentragwerke im Wellenzahlbereich und Prognose der abgestrahlten Schallleistung, in Lehrstuhl fuer Baumechanik. 2012, Technische Universitaet München.

[5] ISO 16283-2:2015, Acoustics – Field measurement of sound insulation in buildings and of building elements – Part 2: Impact sound insulation

[6] ISO 15186-1:2000, Acoustics – Measurement of sound insulation in buildings and of building elements using sound intensity – Part 1: Laboratory measurements

[7] Jacobsen, F., Fundamentals of Acoustic and Noise Control, Lecture note, 2005, DTU.

[8] Vigran, T.E., Building Acoustics. 2008: Taylor and Francis.

[9] Homb, A., C. Guigou-Carter, and A. Rabold, Impact sound insulation of cross-laminated timber/massive wood floor constructions: Collection of laboratory measurements and result evaluation. Building Acoustics, 2017. 24(1): p. 35-52.

[10] Berner Fachhochschule, Prüfbericht A2. Def 4.1, 2013